Proceedings World Geothermal Congress 2020+1
Reykjavik, Iceland, April - October 2021

Numerical Investigation of Hydraulic Stimulation in Pohang Fractured Geothermal Reservoir, South Korea

Márton Pál Farkas, Hannes Hofmann, Günter Zimmermann, Arno Zang

Helmholtz Centre Potsdam GFZ German Research Centre for Geosciences, Telegrafenberg, 14473 Potsdam, Germany

Falko Bethmann and Peter Meier

Geo-Energie Suisse AG, Reitergasse 11, 8004 Zürich, Switzerland

farkas@gfz-potsdam.de

Keywords: Enhanced Geothermal System, Pohang geothermal reservoir, hydraulic stimulation, FracMan

ABSTRACT

In this study, we investigate numerically the hydro-mechanical behavior of fractured crystalline rock due to hydraulic stimulation at the Pohang Enhanced Geothermal site in South Korea. Several hydraulic stimulations were performed in wells PX-1 and PX-2. We use the commercial code FracMan (Golder Associates) that enables studying dynamic hydro-mechanical coupled processes in fractured media in three dimensions combining the finite element method with a discrete fracture network. The software is used to simulate fluid pressure perturbation and related stress redistribution at fractures during hydraulic stimulation. Our numerical simulation shows that pressure history match can be obtained by partitioning the treatment into separate phases. The simulated extent of the 0.01 MPa overpressure contour at the end of the treatment equals to ~180 m around the injection point.

1. INTRODUCTION

The Enhanced Geothermal System (EGS) technology is in the focus of geothermal energy research due to its large economic growth potential (Rybach, 2014). The target is the heat stored in the deeper Earth's crust at several km depth which may be utilized for heat and/or electric power provision. Under petrothermal conditions, i.e. rock with low intrinsic permeability, hydraulic stimulation is essential to increase productivity. However, man-made or induced earthquakes associated with such operations pose a potential risk that must be controlled to advance the EGS technology (Zang et al., 2013). Therefore, the goal is to create a permeable fracture network for an efficient heat exchanger by injecting fluid with induced seismicity at acceptable levels.

The concept of cyclic injection with the aim to enhance permeability and reduce the magnitudes of the largest induced seismic events was introduced by Zang et al., 2013. The concept has been demonstrated experimentally in recent years at different scales: at laboratory (cm) scale by Zhuang et al., 2018 and at mine (dm) scale by Zang et al., 2017. The concept has been demonstrated at field scale by Hofmann et al., 2019 at the Pohang EGS site in South Korea. One may analyze and so improve the concept by using hydro-mechanical coupled numerical codes that provide better understanding of the interrelations between stress field, fluid diffusion and fracturing processes (Yoon et al., 2014).

In this study, we use the 3D finite element software FracMan (Golder Associates, 2019) to investigate the relevant coupled processes in detail. The code uses the Discrete Fracture Network (DFN) approach that combines continuum and discontinuum geomechanics. We focus on studying coupled processes using the dataset of soft stimulation performed by Hofmann et al., 2019 in August 2017 to characterize the fractured crystalline reservoir.

This paper first characterizes the site. This is followed by presenting the numerical model setup. Simulation results are analyzed and discussed, and finally, conclusions are drawn.

2. POHANG EGS PROJECT

The EGS pilot site is located several kilometers north of the city of Pohang, in the SE part of South Korea (Figure 1). A local geological model is presented by Lee et al., 2015 and Park et al., 2017a. The host reservoir rock is fractured Permian granodiorite and granitic gneiss that form the bedrock of the Heunghae Basin below 2200 m depth (Figure 2). This is covered by Cretaceous sedimentary rock (sandstones and mudstones) mixed with sequences of tuff and andesite layers, with a thickness of 1000 m. The uppermost Tertiary semi-consolidated mudstone shows a varying thickness of 200 m in the northern part which increases up to 400 m to the south.

The basin is bounded on the west by the Yangsan fault which is characterized by post-Eocene dextral strike–slip movement (Chough et al., 2000). The regional fault strikes NNE-SSW, passing approx. 10 km west of the Pohang site. The EGS site is intersected by two sets of faults (Figure 3). One set, the Gokgang fault zone, is oriented NNE-SSW and is described as a steeply dipping, right-lateral strike-slip branch of the regional Yangsan fault. The Heunghae fault zone is oriented approx. E-W and intersects the other set perpendicularly. The Heunghae fault set consists of normal faults.

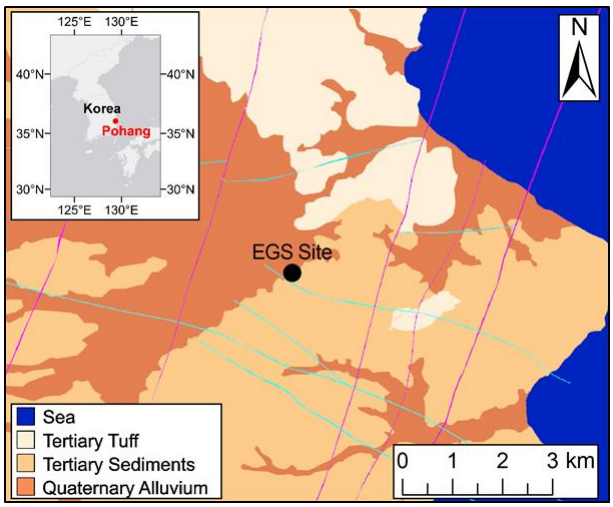

Figure 1: Surface geologic layers and fault structures at the Pohang EGS site in South Korea (Hofmann et al., 2019)

The stress field is based on the rock stress model established by Kim et al., 2017 and Park et al., 2017a (Table 1). The model is based on hydraulic fracturing and borehole breakout data of well EXP-1, which is located approx. 4 km from the Pohang EGS project site. The stress model suggests that the site is located in a strike-slip regime with S_{Hmax} orientation varying between NEE-SWW and NWW-SEE.

Table 1: Stress model of the Pohang EGS reservoir (based on Park et al., 2017a)

	S_{Hmax} orientation (°)	S_{Hmax} (MPa)	S_v (MPa)	S_{hmin} (MPa)	Stress Regime
Stress model for 4.2 km depth	N65-130E	115-140	110	82-105	Strike-slip

Two wells were drilled for an anticipated doublet system (Figure 2). Well PX-1 was drilled and side-tracked to a measured depth of 4362 m (true vertical depth: 4215 m) with an 8 ½" open hole section of 313 m length at the bottom of the hole. The well PX-2 was drilled vertically down to 4348 m with a 140 m long 8 1/2" open hole section. On the surface the wells are 6 m apart. The horizontal distance at the bottom level of the wells is 616 m.

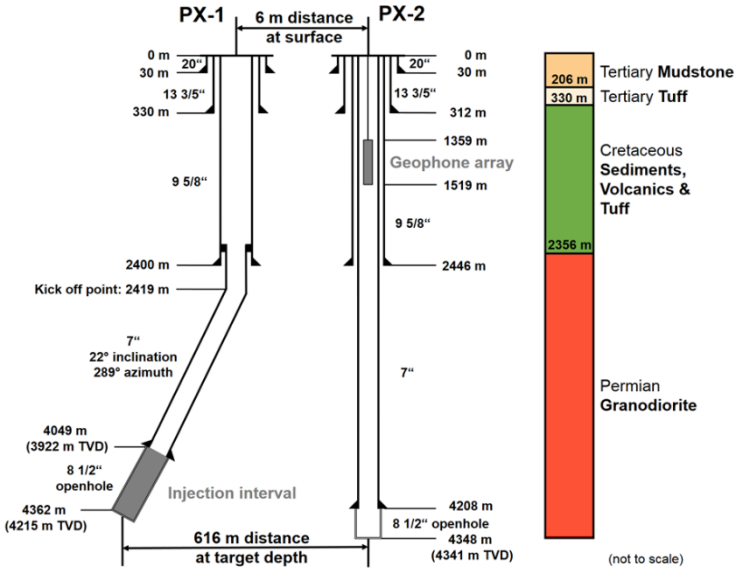

Figure 2: Well completions including injection location (PX-1, 313 m long openhole section from 4,049 m to 4,362 m MD) and 17-instrument geophone chain (installed in well PX-2, at 1,359 m – 1,519 m MD, to monitor the August 2017 stimulation in well PX-1). Depth reference is the rig floor, 26.3 m above sealevel and ~9 m above surface (Hofmann et al., 2019)

Before and after the stimulation in well PX-1 in August 2017, several hydraulic stimulations were performed in the two wells in the past years to improve the hydraulic performance of the doublet system (Hofmann et al., 2019). During the cyclic soft stimulation treatment the largest magnitude event was below the anticipated target threshold of M_w=2.0, however, no significant and sustainable productivity increase was achieved probably due to the limited size of the treatment (Figure 3, Hofmann et al., 2019). The well tests in PX-1 imply hydro-shearing supported by critical stress analysis and injectivity development (Park et al., 2017b). The hydraulic injections in well PX-2 imply hydraulic fracturing as main process for increased injectivity and relatively high wellhead pressures (Park et al., 2017a). For more information on the Pohang EGS pilot project and the hydraulic stimulation treatments, the reader is referred to Hofmann et al., 2019 and Lee, 2019.

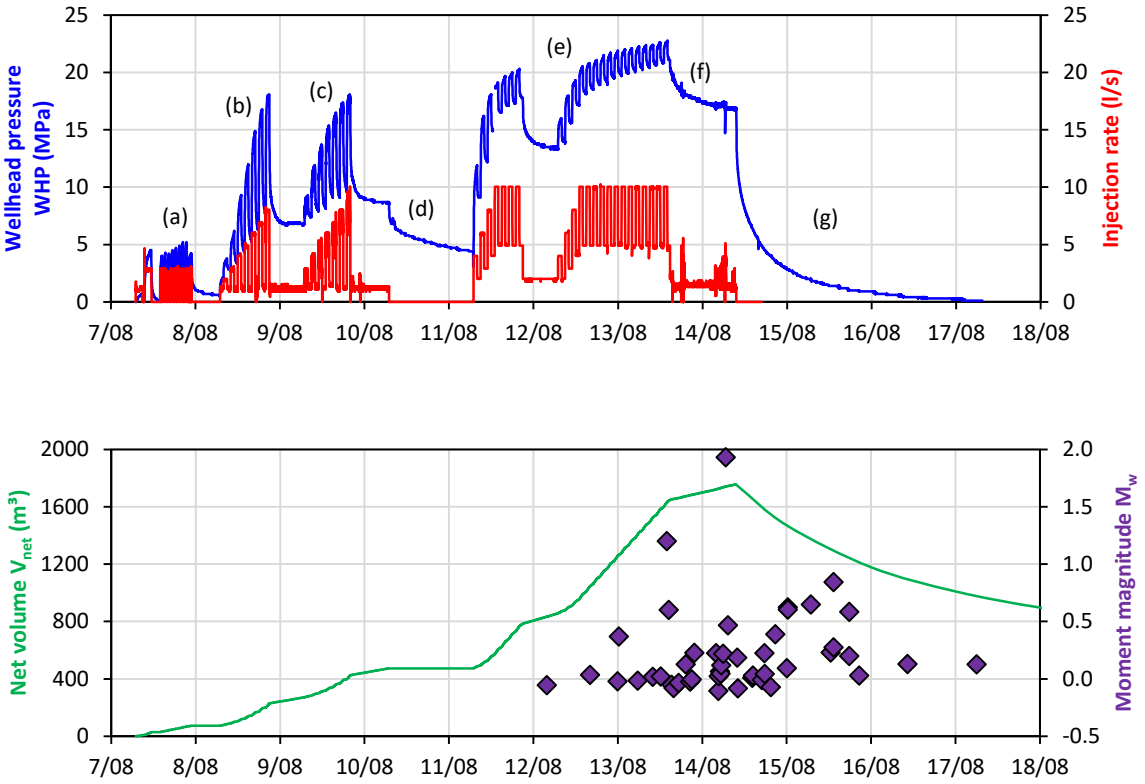

Figure 3: Overview of well head pressure (WHP), injection rate (Q), injected net volume (V_{net}), and moment magnitude M_w of induced seismic events during the August 2017 CSS treatment in well PX-1. This treatment can be divided into seven phases: (a) Day 1: initial injectivity determination, (b) Day 2: fracture opening pressure determination, (c) Day 3: hydraulic pulse tests, (d) Day 4: shut-in, (e) Days 5 through 7: main cyclic soft stimulation treatment, (f) Days 7 through 8: pressure reduction due to orange traffic light alert, and (g) complete flow back due to red traffic light alert. (Hofmann et al., 2019).

The joint interpretation of well test and microseismic data implies two fault structures (Figure 4). One fault, which is referred to as plane P1, intersects the open hole section of well PX-1. It is assumed to be the main conductive structure as well as the plane for hydro-shearing. The other structure, plane P2, intersects the cased part of well PX-2 at approx. 3800 m MD and contains the hypocenter of M_w 5.5 earthquake event.

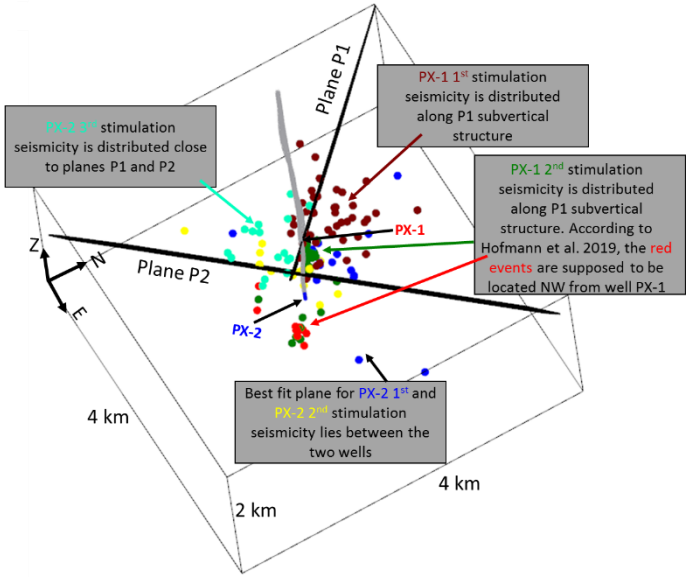

Figure 4: Joint structural interpretation of hydraulic data and microseismic clouds of PX-1 and PX-2 hydraulic stimulations (Modified from Bethmann et al., 2019).

3. NUMERICAL MODEL

3.1 Numerical Method

The hydro-mechanical behavior of the stimulated fractures is simulated through an explicit, iterative process described below. The coupling concerns the description of stress-aperture relationships according to Barton et al., 1985. Their empirical equation for estimating the initial mechanical aperture, E_0, at low stress levels is based on the measured values of *JRC* and *JCS*:

$$E_0 = \frac{JRC}{5}\left(0.2\frac{UCS}{JCS} - 0.1\right) \tag{1}$$

Where *JRC* is joint roughness coefficient, *UCS* is the uniaxial compressive strength and *JCS* is joint wall compression strength. Note that the equation units are important. E_0 must be in mm, *UCS* and *JCS* must both be in MPa units. JRC is dimensionless. The changes in mechanical aperture (ΔE) with normal stress (σ_n) is calculated as

$$\Delta E = \frac{\sigma_n V_m}{V_m K_n + \sigma_n} \tag{2}$$

where V_m is the maximum aperture closure and K_n is the fracture normal stiffness. The residual mechanical aperture, *E*, is provided by the equation:

$$E = E_0 - \Delta E \tag{3}$$

Hydraulic or fluid conducting aperture, *e*, can be estimated from mechanical aperture *E* and *JRC* as

$$e = \frac{E^2}{JRC^{2.5}} \tag{4}$$

It must be noted that *E* and *e* are in μm unit. The strength of fracture or fault is provided by the Mohr-Coulomb fracture shear strength criteria:

$$\tau = C_0 + \sigma_n \tan\left(\phi_f\right) \tag{5}$$

Where τ is the shear strength acting in the plane of fracture surface, C_0 is the cohesion of the fracture and ϕ_f is the friction angle. For more details on the numerical method the reader is referred to Cottrell et al., 2016.

Rock stress and strain are treated in rectangular grid cells. These are calculated using Golder's FracStress code package. This code uses a finite element model (FEM) with nodes corresponding to the vertices of the grid cells, and tetrahedral elements, several per grid cell. Each grid cell has material properties that are shared by all the tetrahedral elements that make up the cell. FracStress calculates stresses in a grid based on (far-field) boundary conditions, material properties, and strain field.

The hydraulic part of the simulation is modelled by Golder's Matrix/Fracture Interaction (MAFIC) code. The program models fracture flow through a network of interconnecting fracture element plates and matrix flow through a three-dimensional volume. Flow in fracture is simulated in three-dimensional network of two-dimensional triangular finite elements, assuming incompressible fluid, using the equation of Bear, 1972:

$$S\frac{\partial P}{\partial t} - T\nabla^2 P = q \tag{6}$$

Where *S* is fracture storativity, *P* is fluid pressure, *t* is time, *T* is fracture transmissivity, *q* is source or sink term and ∇^2 is Laplace operator.

Flow in the matrix is simulated by a generic matrix block scheme. The matrix block approach here defines a single, rectangular slab block geometry. This represents all matrix blocks in a network of surrounding fractures. The slabs have a surface area of the drainage face, which is set equal to the fracture element area.

Flow through each matrix block, i.e. between fracture faces, is treated as a one-dimensional pipe flow coupled to the pressure in the associated bounding fracture element:

$$S_S\frac{\partial P}{\partial t} - K\nabla^2 P = q \tag{7}$$

Where S_s is rock specific storage, *P* is fluid pressure, *t* is time, *K* is hydraulic conductivity, *q* is source or sink term and ∇^2 is Laplace operator.

FracMan allows the conversion between the hydraulic simulation parameters transmissivity, storativity and aperture ("TSA") and permeability, compressibility and aperture ("PCA") using the following relationships:

$$\boldsymbol{T_{frac} = \frac{\rho_{fluid} g e^3}{12 \eta_{fluid}}} \tag{8}$$

Conversion between fracture storativity and compressibility is calculated as:

$$\boldsymbol{S_{frac} = \left(C_{frac} + C_{fluid}\right) \rho_{fluid} g e} \tag{9}$$

Conversion between matrix storativity and compressibility is considered as:

$$S_m = \left(C_m + C_{fluid}\right) \rho_{fluid} g \varphi \tag{10}$$

where,

T_{frac} is the fracture transmissivity, respectively;

S_{frac} and S_m are fracture and matrix storativity, respectively;

C_{frac}, C_m and C_{fluid} are fracture, matrix and fluid compressibility, respectively;

η is fluid viscosity;

g is acceleration of gravity; and

φ is matrix porosity.

The hydro-mechanical processes during simulation of fluid injection into a borehole with a given flow rate are realized with the following looping. The elevated pore pressure modifies effective normal stress at and around the injection point. This provides update to fracture aperture that impacts transmissivity, storativity as well as rock strain in three dimensions. Eventually, change in rock strain affects in-situ stresses.

3.2 Numerical Model Setup

The FracMan code allows considering fractures (faults) and intact background rock (host media) explicitly. Fractures are essential for possible flow path, and the background rock is important for defining the rock mechanical properties and stress state. The 3D volume of interest, which contains the faults and the intact background rock, is centered at the PX-1 open borehole section. To ensure independence of boundaries, the model dimensions are 4 km x 4 km x 2 km.

The geometry of the fault planes, P1 and P2, are based on joint interpretation of hydraulic and microseismic information illustrated in Figure 4. Plane P1 strikes NW-SE (N135°E) and dips at 78°. The plane intersects the open hole section of well PX-1 at 4050 m MD, i.e. at the top of the interval. Plane P2 shows strike of SW-NE (N222°E) and dip angle of 61° (Bethmann et al., 2019).

The grid representing the intact rock considers the crystalline rock strength and the input for defining the in-situ stress field as spatially-variable grid properties (Figure 5). The size of the grid elements is set to 100 m x 100 m x 100 m, and 32000 grid cells are generated in total. These ensure numerical stability and acceptable computational time. The geomechanical model properties are summarized in Table 2 and Table 3.

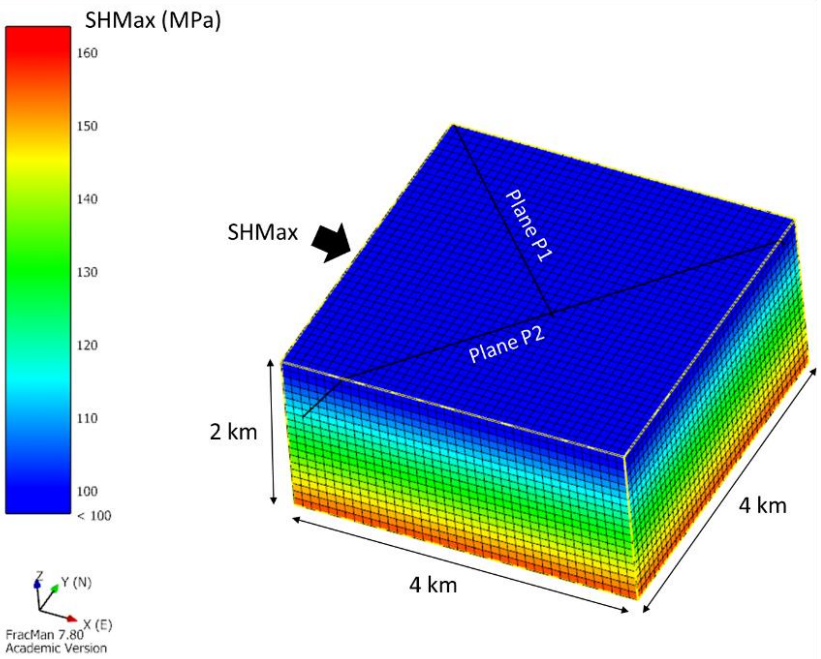

Figure 5: Oblique view looking down from NE illustrating the grid showing the spatial distribution of maximum principal stress with the Fault planes, P1 and P2 (*black* lines). The modelling box dimensions are 4 km x 4 km x 2 km. Grid element dimensions are 100 m x 100 m x 100 m

Table 2. Target Granodiorite Geomechanical Parameters (Kwon et al., 2019)

Geomechanical Property of Intact Rock	Mean Value	Standard deviation	Number of tests
Bulk Density (kg/m^3)	2630	5	11
Porosity (%)	0.5	0.07	11
Uniaxial Compressive Strength, UCS (MPa)	106.7	22.3	7
Tensile Strength (MPa)	9.2	0.4	2
Young's Modulus (GPa)	33.5	6.8	4
Poisson's Ratio	0.21	0.05	4
Cohesion (MPa)	15.2	-	12

Table 3: Geomechanical Properties of Fractures Derived from Laboratory Tests (Kwon et al., 2019)

Geomechanical Property of Fracture	Mean Value	Standard deviation	Number of tests
Joint Wall Compressive Strength, JCS (MPa)	169.2	87.2	5
Joint Roughness Coefficient, JRC (-)	13.1	2.8	7
Friction Angle of Fracture (°)	26.6	0.5	2

Table 4 specifies the strike-slip stress field parameters (based on Table 1**)** with the gradients for minimum horizontal stress (S_{hmin}), vertical stress (S_v) and maximum horizontal stress (S_{Hmax}) as well as pore pressure, assuming a fluid density of 1000 kg/m³ and a gravitational acceleration of 9.81 m/s².

Table 4. Rock Stress Parameters used for the numerical study

Parameter	Value
Maximum Horizontal Stress Gradient, S_{Hmax} (MPa/m)	0.0317
Vertical Stress Gradient, S_v (MPa/m)	0.0258
Minimum Horizontal Stress Gradient, S_{hmin} (MPa/m)	0.0227
S_{Hmax} Direction (°)	N100E
Fluid Pore Pressure Gradient (MPa/m)	0.00981

3.3. Simulation of PX-1 2nd hydraulic stimulation

In the model, fluid is injected into the P1 fault plane over eight days with varying flow rates following the injection protocol in Hofmann et al., 2019. Prior to simulation, the fault planes are meshed into triangular elements with a minimum edge length of 0.1 m and maximum edge lengths of 75 m, 40 m, 30 m, 25 m and 20 m to avoid mesh-dependency. The minimum length is similar to the radius of well PX-1; and the maximum size is similar to that of matrix grid elements. The mesh is refined close to the node representing the borehole area and consists of 25650, 48367, 78679, 107894 and 153522 nodes for meshes with maximum edge length of 75 m, 40 m, 30 m, 25 m and 20 m, respectively. The injection into the plane is simulated using a source term (node) at the intersection of

the open borehole section of well PX-1 and P1. An initial unperturbed hydrostatic pore pressure conditions is specified. Pressure increase from static level due to fluid injection is referred to as overpressure. The validation of the model is performed by matching the simulated wellhead pressure history against field observations. The matching period begins at the onset of injection and lasts until the onset of the flowback phase. The simulated injection flow rates are identical to those recorded in the field. The validation procedure requires adjusting the input parameters governing the hydro-mechanical coupling sequentially. These are referred to as breakpoints dividing the simulation into sequences. At the time of change in parameters, the pressure output of the last time step is taken as input for the subsequent phase of the simulation. These parameters remain valid for a period until the next breakpoint is defined. In total, 6 breakpoints, i.e. sequences are defined in the simulation.

Properties that are assumed to be constant include well radius, fluid and matrix properties, wellbore compressibility, fault compressibility as well as geomechanical properties except for UCS are summarized in Table 5.

Table 5: Fluid injection (well effect and fluid), hydrogeological (matrix and fault) and geomechanical properties of the numerical simulation of cyclic soft stimulation (CSS) treatment in well PX-1 in August 2017

Fluid injection parameters		Reference/Remark
Well radius, r_{well} (m)	0.108	Hofmann et al., 2019
Well storage coefficient (m^3/Pa)	$6\ 10^{-8}$	Product of borehole volume and fluid compressibility
Fluid properties		
Fluid viscosity, η_{fluid} (mPa s)	0.3	Hofmann et al., 2019
Fluid compressibility, C_{fluid} (1/Pa)	$4.5\ 10^{-10}$	
Fluid density, ρ_{fluid} (kg/m^3)	1000	
Matrix properties		
Matrix permeability, k_m (m^2)	$1.8\ 10^{-16}$	Hofmann et al., 2019
Porosity, φ (%)	0.5	Kwon et al., 2019
Matrix compressibility, C_m (1/Pa)	$4.5\ 10^{-10}$	
Numerical block radius, r (m)	15	
Fault hydrogeological property		
Fault compressibility, C_{frac} (1/Pa)	$4.5\ 10^{-10}$	
Fault geomechanical properties		
Normal stiffness, K_n (GPa/m)	200	Yoon et al., 2014
Coefficient of friction, μ (-)	0.23	Critical stress analysis in Section 3.2
JRC (°)	12	Kwon et al., 2019
JCS (MPa)	105	Kwon et al., 2019
Maximum closure, κ (mm)	1	

4. RESULTS

We present and analyze the results for separate days of the treatment. The injection protocol and the pressure response are summarized briefly, and the simulated results are discussed afterwards for each respective day.

The simulated and recorded pressures are illustrated in Figure 6. The adjusted numerical parameters of the simulations are summarized in Table 6. Figure 7 shows the simulated pressure dependent aperture and transmissivity.

4.1 Day 1: Initial injectivity determination

The first day of the treatment focused on determination of the initial reservoir conditions. The stimulation program included a 2-hour-long injection with constant flow rate of 3 l/s, followed by a 2-hour shut-in phase. Afterwards, cyclic test with eight 1-hour cycles with periods of 30 minutes of 3 l/s injection and 30 minutes of shut-in were performed. This phase served as comparison with the conventional 2-hour injection test. At the end of the day, ten 6-minute cycles with the same flow rates were conducted. The maximum WHP reached 4 MPa at the end of the last test.

The simulated WHP response shows good match with the recorded one. At static pore pressure, marked as split-point ID 1, the hydraulic aperture is 0.06 mm at the wellbore corresponding to transmissivity of $7.5\ 10^{-7}$ m^2/s.

4.2 Day 2: Fracture opening pressure determination

The second day of the treatment aimed at determining the fracture opening pressure by a progressive cyclic injection test. This was realized by seven 2-hour cycles with 1 l/s base injection rate. The injection rate was progressively increased from 2 l/s to 8 l/s with 1 l/s steps. The maximum WHP was 18 MPa, which lies in the range of hydro-shearing.

To achieve a reasonable match of the pressure curves, an additional split-point ID 2 is inserted. The split-point is set before the pressure curve reaches the critical pressure range for deformation, i.e. 16-18 MPa, interpreted as hydro-shearing at increased flow rates (Hofmann et al. 2019). This is captured by modifying the stress-aperture relationship by increasing the UCS within the range

shown in Figure 11. The hydraulic aperture, therefore, increases from 0.06 mm to 0.08 mm. Transmissivity increases from 7.5 10^{-7} m^2/s to 1.8 10^{-6} m^2/s.

4.3 Day 3 and day 4: Hydraulic pulse tests and Shut-in

On the third day harmonic pulse tests (referred also to as cyclic progressive pulse test) were performed by adding pulses on top of the high rate injections. The flow rates are chosen to ensure the same injected volume and average injection rate during all cycles in both progressive cyclic injection test and hydraulic pulse tests. Injection was continued at the 1 l/s base rate until day 4 with a similar length as the previous test. On day 4, the well was kept shut-in for 24 hours. This allowed observing the hydraulic and seismic behavior of the system. The wellhead pressure reached up to 18 MPa and dropped from 9 MPa to 4.5 MPa during the shut-in phase.

The simulated WHP can be matched against field record if an additional split-point is inserted during the phase of increasing flow rates. This split-point ID 3 is defined at WHP of 9.30 MPa, just before the critical pressure for hydro-shearing is reached at the following higher injection rate. At this split-point the UCS is further increased corresponding to hydraulic aperture increase to 0.11 mm and transmissivity increase to 3.6 10^{-6} m^2/s.

The simulated wellhead pressure matches with the field record using the latest hydro-mechanical parameters until the onset of the shut-in period. The simulation phase starting at ID 4 is defined at the beginning of the shut-in phase. At this point, the UCS is reduced which results in decreased hydraulic aperture and transmissivity at the injection point, 0.08 mm and 2 10^{-6} m^2/s, respectively. This can be explained with pressure drop well below the range for hydro-shearing. This simulation period lasts until the end of day 4. The variations in parameters at split-points ID 3 and 4 mimic fracture opening and closure for this period.

Table 6: Adjusted fault geomechanical property of the numerical simulation of cyclic soft stimulation (CSS) treatment in well PX-1 in August 2017

	Day 1	Day 2	Day 3 – Day 4		Day 5	Day 6 – Day 8	
Split-point ID	1	2	3	4	5	1	2
UCS (MPa)	103	108	113	109	110	103	108

4.4 Day 5: Main cyclic soft stimulation phase

The main cyclic soft stimulation treatment began on day 5. Injection lasted for 14 hours with cycles of 2 hours length. The high injection rate during the cycling equals to 10 l/s and the low one is 5 l/s. This was followed by 10 hours of base rate injection of 2 l/s overnight. The highest observed WHP was 20 MPa.

The simulation of injection begins with defining split-point ID 5 at WHP 4.5 MPa before the phase of increasing flow rates resulting in WHP larger than the pressure for hydro-shearing. The split-point is required in order to achieve an acceptable match between observed and simulated pressure record. At the end of Day 5, the WHP decreases below hydro-shearing pressure. At split-point ID 5, the UCS is increased again. The resulting hydraulic aperture is 0.095 mm and the transmissivity is 2.3 10^{-6} m^2/s.

4.5 Days 6 and 7: Continuation of main cyclic soft stimulation phase. Flow rate and pressure reduction due to microseismic alert

The main cyclic soft stimulation phase was extended for days 6 and 7. Confidence for continuation was gained by the lack of seismic activity detected so far at the stimulation program. Furthermore, this also contributed to data acquisition that could be used for hydraulic pulse test analysis. In this period, the injection schedule was the same as on the previous day, except for seven more repetitions of the cycle of 5-10 l/s (Salina Borello et al., 2019). The maximum WHP reached 22.8 MPa, which equals to the absolute maximum WHP for the treatment.

Due to occurrence of M_w 1.2 microseismic event (which was first analyzed as an event with M_w 1.4), the injection rate was decreased stepwise to 2 l/s, then to 1 l/s. 15 microseismic events with magnitude below M_w 1.0 were observed in this period (Figure 3).

The history matching of the pressure curve requires inserting a split-point at the beginning of day 6. At time point ID 6, where the WHP is 13.6 MPa, the UCS is increased to mimic increase in hydraulic aperture and transmissivity. The calculated hydraulic aperture and transmissivity equal 0.12 mm and 5 10^{-6} m^2/s. The split-point is inserted just before the critical pressure for hydro-shearing is reached again at the subsequent higher injection rate.

4.6 Day 8: Continuation of flow rate and pressure reduction. Complete flowback

On the last day of main cyclic soft stimulation phase, the injection with 1 l/s went on until the detection of event M_w 1.9. After analyzing the microseismic event, the injection was stopped and the well was opened for flowback. Several events were detected during, and after this period with M_w around or less than 1.0. The maximum WHP was 18 MPa.

The history matching of wellhead pressure is achieved via continuing the simulation with the parameters defined at split-point ID 6. This might be related to the evolution of WHP which is above the pressure for hydro-shearing until the flowback period.

In Figure 8, the extent of pressurized subsurface area is plotted at WHP of 17.1 MPa, just before complete flowback at last time step. The pressurized area, i.e. direct pore pressure change that may be linked to induced microseismic events within fault P1 shows that the extent of overpressure of 0.01 MPa, threshold defined by Lee et al., 2019, in the direction of the shortest possible distance to the plane P2 is approx. 180 m. The hydraulic diffusion reaches as far as 450 m, i.e. the overpressure goes beyond the intersection between P1 and P2. However, the magnitude of overpressure on P2 is below 0.01 MPa.

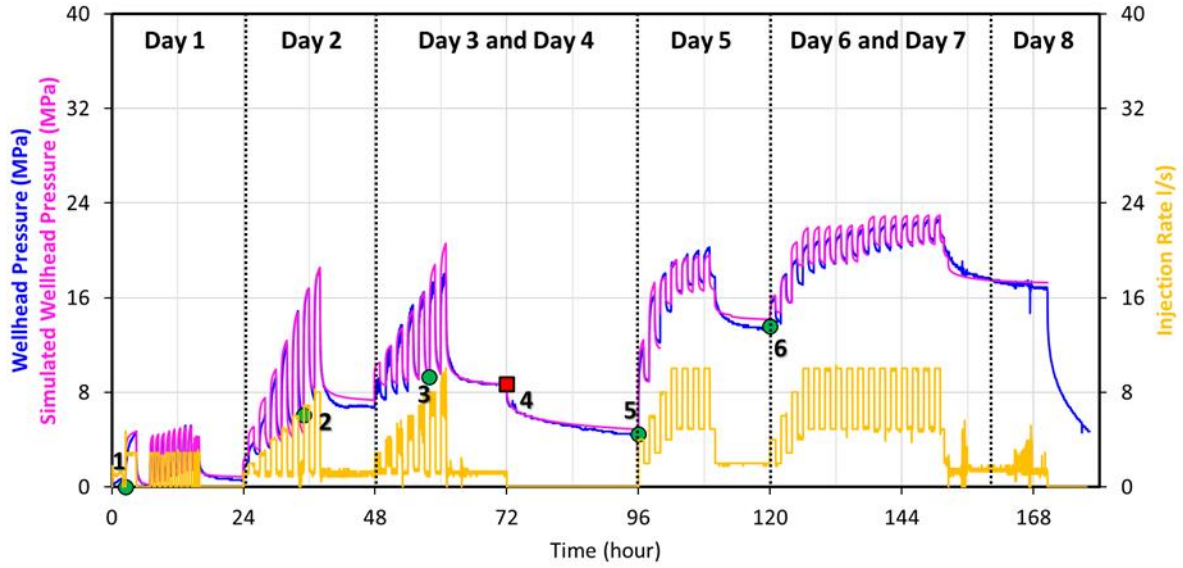

Figure 6: Comparison of recorded (*pink*) and modelled (*pink*) wellhead pressure data for cyclic soft stimulation (CSS) treatment in well PX-1 of August 2017. Numerical injection flow rates are equal to that recorded on field (*yellow*). *Light green* circles represent increase in hydraulic aperture. *Red squares* represent decrease in hydraulic aperture

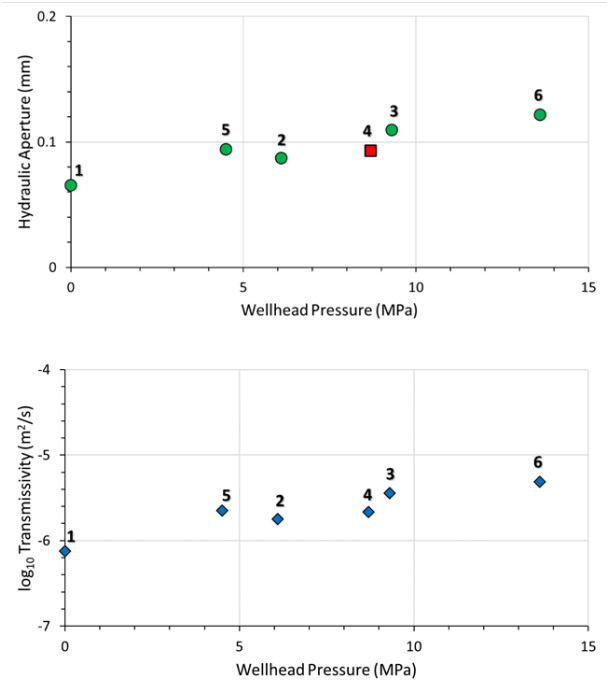

Figure 7: Top: simulated hydraulic aperture development with wellhead pressure. Bottom: simulated transmissivity (blue diamond) development with wellhead pressure. The IDs 1 through 6 represent split-points, i.e. change in input parameters, as shown in Table 6 and Figure 6. The order of IDs increases with stimulation time

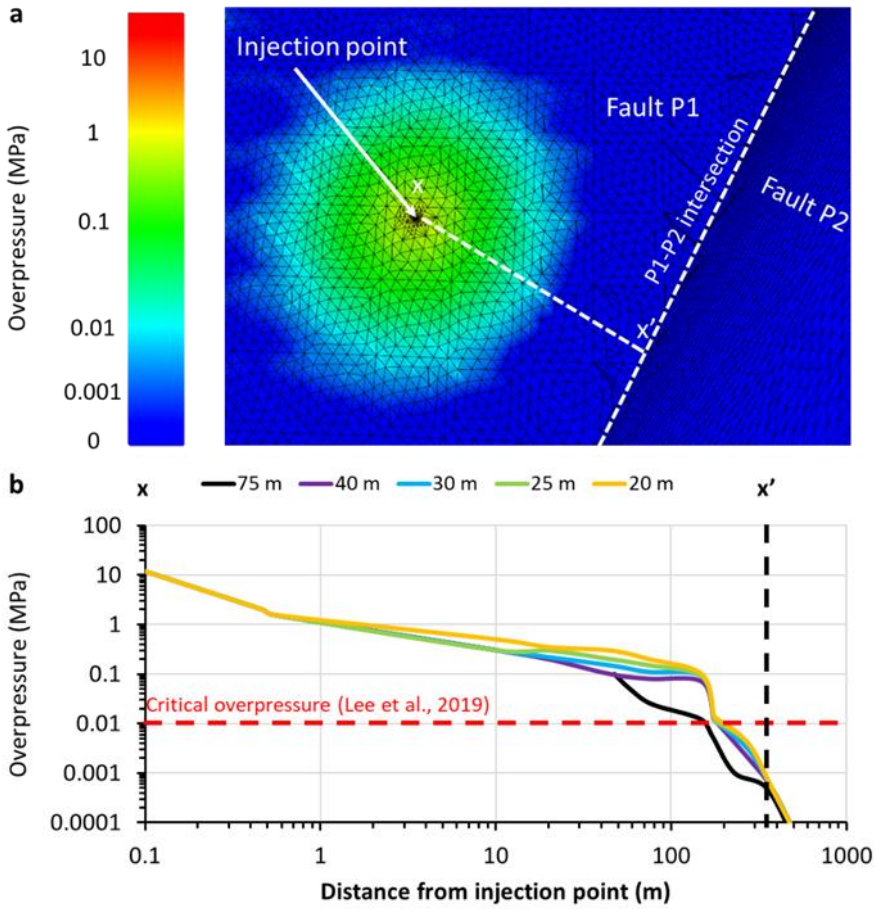

Figure 8: The extent of pressurized subsurface area (investigation radius) at the end of the August 2017 stimulation in well PX-1 before flowback. (a): View is looking obliquely down from the NE. The largest edge length is 75 m. The smallest edge length is 0.1 m. (b): overpressure profile along section x-x'. The red dashed line denotes the critical overpressure level of 0.01 MPa defined by Lee et al., 2019 for potential induced seismic event. In order to eliminate bias due to mesh-dependence, the extent of overpressure is shown for different maximum mesh edge lengths, i.e. 75 m, 40 m, 30 m, 25 m as well as 20 m.

5. DISCUSSION

The simulation of August 2017 stimulation in well PX-1 shows that the fluid diffusion due to hydraulic stimulation is governed by several parameters. The wellbore storage, hydro-mechanical coupling (stress versus hydraulic aperture relationship) and fault permeability have strong effect on the simulated wellhead pressure.

Wellbore storage coefficient requires fluctuation of one order of magnitude, implying strong borehole effect throughout the stimulation. The fault permeability is varied over an order of magnitude suggesting fracture opening. The hydraulic aperture variation is captured by modified stress-aperture relationships. This is done by varying UCS throughout the simulation as its variation allows slight shift of the stress-aperture curve.

Both hydraulic stimulations in well PX-1 shows characteristic change in injectivity at WHPs between 15 and 17 MPa. Based on critical stress analysis of Park et al., 2017b, this phenomenon is linked to hydro-shearing. However, it can be argued that the simulated hydraulic aperture development resembles hydraulic jacking, i.e. hydraulic fracturing of existing fractures (Doe and Korbin, 1987). This is characterized by reversible, elastic aperture opening and closing with pressure below critical pressure level. Furthermore, the calculated hydraulic apertures agree with that in Park et al., 2017b. Hence, we do not observe any permanent increase in hydraulic aperture in fault P1.

The extent of directly pressurized fault radius of 180 m with 0.01 MPa cut-off value implies that the hydraulic diffusion for inducing seismic events is limited relatively close to near-well area during the time of injection. This is demonstrated by the pressure distribution around the injection point in Figure 8b. Given that the simulated injection point is located approx. 350 m as shortest distance from plane P2 along P1 (Figure 8), the modelling results reveal that the pore pressure, and thus, the effective stresses at fault P2 are changed only by less than 0.001 MPa during the treatment.

The presented results represent a first attempt to model the hydraulic stimulation treatment in Pohang in August 2017 using the software FracMan. Due to several reasons the model will be updated in the future. First, the change in stress versus hydraulic aperture relationship over time implies that this behavior during the treatment either cannot be characterized by a single law or a different equation may be utilized. Different stress versus aperture relationships should be tested in a future study. Second, the model does not include temperature dependent fluid properties. Third, the model does not include the effects of the stimulations and flowback periods

performed before and after the August 2017 stimulation in the two wells. This data needs to be included in order to evaluate the full hydraulic history of the site.

6. CONCLUSIONS

We investigated the hydro-mechanical behavior of a fault that crosses the open borehole section of well PX-1 at the Pohang EGS site. The August 2017 cyclic soft stimulation treatment, second stimulation in the well, was simulated in three dimensions using the FracMan code. The numerical wellhead pressure was validated against the field record. Our study draws the following conclusions:

1. With our model, a reasonable history match of the wellhead pressure could only be achieved by partitioning the treatment into separate periods. Partitioning the stimulation is beneficial computationally. Furthermore, it can capture phenomena related to fracture opening and closing, i.e. change in hydraulic aperture that are otherwise not captured by the code.
2. The hydraulic aperture evolution is typical of hydraulic fracturing. However, the fault is favorably oriented for hydro-shearing, which is generally characterized by permanent increase in aperture. This is explained by permeability increase through opening of the existing fault.
3. The influence of the treatment until flowback, i.e. the extent of direct pore pressure difference of >0.01 MPa is approx. 180 m in the direction of the shortest possible distance to the plane P2 along plane P1. This is half way between the injection and the plane of interest.

ACKNOWLEDGEMENTS

The DESTRESS project has received funding from the European Union's Horizon 2020 research and innovation program under grant agreement No 691728. First and second author are funded by this project.

REFERENCES

Barton, N., Bandis, S., Bakhtar, K., 1985. Strength, deformation and conductivity coupling of rock joints. International Journal of Rock Mechanics and Mining Sciences & Geomechanics Abstracts 22(3), 121-140.

Bear, J., 1972. Dynamics of Fluids in Porous Media. American Elsevier Publishing Company, New York.

Bethmann, F., Ollinger, D., Tormann, T., Heimlich, C., Meier, P., 2019. Seismicity Analysis of the Pohang EGS Project, Proceedings World Geothermal Congress 2020. Reykjavik, Iceland.

Chough, S.K., Kwon, S.T., Ree, J.H., Choi, D.K., 2000. Tectonic and sedimentary evolution of the Korean peninsula: a review and new view. Earth-Science Reviews 52(1), 175-235.

Cottrell, M., Hosseinpour, H., Dershowitz, W., 2016. Deep Fluid Injection into Fractured Rock, 50th US Rock Mechanics / Geomechanics Symposium. American Rock Mechanics Association, Houston, Texas, USA.

Doe, T.W., Korbin, G.E., 1987. A Comparison Of Hydraulic Fracturing And Hydraulic Jacking Stress Measurements, The 28th U.S. Symposium on Rock Mechanics (USRMS). American Rock Mechanics Association, Tucson, Arizona, p. 8.

Golder Associates, 2019. FracMan Interactive Discrete Feature Data Analysis, Geometric Modeling and Exploration Simulation, User Documentation, v7.8.

Hofmann, H., Zimmermann, G., Farkas, M., Huenges, E., Zang, A., Leonhardt, M., Kwiatek, G., Martinez-Garzon, P., Bohnhoff, M., Min, K.-B., Fokker, P., Westaway, R., Bethmann, F., Meier, P., Yoon, K.S., Choi, J.W., Lee, T.J., Kim, K.Y., 2019. First field application of cyclic soft stimulation at the Pohang Enhanced Geothermal System site in Korea. Geophysical Journal International 217(2), 926-949.

Kim, H., Xie, L., Min, K.-B., Bae, S., Stephansson, O., 2017. Integrated In Situ Stress Estimation by Hydraulic Fracturing, Borehole Observations and Numerical Analysis at the EXP-1 Borehole in Pohang, Korea. Rock Mechanics and Rock Engineering 50(12), 3141-3155.

Kwon, S., Xie, L., Park, S., Kim, K.-I., Min, K.-B., Kim, K.Y., Zhuang, L., Choi, J., Kim, H., Lee, T.J., 2019. Characterization of 4.2-km-Deep Fractured Granodiorite Cores from Pohang Geothermal Reservoir, Korea. Rock Mechanics and Rock Engineering 52(3), 771-782.

Lee, K.-K., 2019. Summary report of the Korean Government Commission on relations between the 2017 Pohang earthquake and EGS project, in: Lee, K.-K. (Ed.) Geological Society of Korea. The Geological Society of Korea, p. 205.

Lee, T.J., Song, Y., Park, D.-W., Jeon, J., Yoon, W.S., 2015. 3D Geological Model of Pohang EGS Pilot Site, Korea, World Geothermal Congress. Melbourne, Australia.

Park, S., Xie, L., Kim, K.-I., Kwon, S., Min, K.-B., Choi, J., Yoon, W.-S., Song, Y., 2017a. First Hydraulic Stimulation in Fractured Geothermal Reservoir in Pohang PX-2 Well. Procedia Engineering 191, 829-837.

Park, S., Kim, K.-I., Xie, L., Yoo, H., Min, K.-B., Choi, J., Yoon, W.-S., Yoon, K., Song, Y., Lee, T.J., Kim, K.Y., 2017b. Hydraulic Stimulation in Fractured Geothermal Reservoir in Pohang PX-1 Well, 4th ISRM Young Scholars Symposium on Rock Mechanics. International Society for Rock Mechanics and Rock Engineering, Jeju, Korea, p. 2.

Rybach, L., 2014. Geothermal Power Growth 1995–2013—A Comparison with Other Renewables. Energies 7(8), 4802-4812.

Salina Borello, E., Fokker, P.A., Viberti, D., Verga, F., Hofmann, H., Meier, P., Min, K.-B., Yoon, K., Zimmermann, G., 2019. Harmonic Pulse Testing for Well Monitoring: Application to a Fractured Geothermal Reservoir. Water Resources Research 0(0).

Yoon, J.S., Zang, A., Stephansson, O., 2014. Numerical investigation on optimized stimulation of intact and naturally fractured deep geothermal reservoirs using hydro-mechanical coupled discrete particles joints model. Geothermics 52, 165-184.

Zang, A., Yoon, J.S., Stephansson, O., Heidbach, O., 2013. Fatigue hydraulic fracturing by cyclic reservoir treatment enhances permeability and reduces induced seismicity. Geophysical Journal International 195(2), 1282-1287.

Zang, A., Stephansson, O., Stenberg, L., Plenkers, K., Specht, S., Milkereit, C., Schill, E., Kwiatek, G., Dresen, G., Zimmermann, G., Dahm, T., Weber, M., 2017. Hydraulic fracture monitoring in hard rock at 410 m depth with an advanced fluid-injection protocol and extensive sensor array. Geophysical Journal International 208(2), 790-813.

Zhuang, L., Kim, K.Y., Jung, S.G., Diaz, M., Min, K.-B., Park, S., Zang, A., Stephansson, O., Zimmermann, G., Yoon, J.S., 2018. Cyclic hydraulic fracturing of cubic granite samples under triaxial stress state with acoustic emission, injectivity and fracture measurements, 52nd US Rock Mechanics / Geomechanics Symposium. Seattle, USA.